

# Nonreciprocal quantum correlations via Barnett effect in molecular optomagnonics

E. Kongkui Berinyuy,<sup>1,\*</sup> A.-H. Abdel-Aty,<sup>2</sup> P. Djorwé,<sup>3,†</sup> M. Abdalla,<sup>4,‡</sup> and K.S. Nisar<sup>5,§</sup>

<sup>1</sup>*Department of Physics, Faculty of Science, University of Yaounde I, P.O.Box 812, Yaounde, Cameroon*

<sup>2</sup>*Department of Physics, College of Sciences, University of Bisha, Bisha 61922, Saudi Arabia*

<sup>3</sup>*Department of Physics, Faculty of Science, University of Ngaoundere, P.O. Box 454, Ngaoundere, Cameroon*

<sup>4</sup>*Department of Mathematics, College of Science,*

*King Khalid University, P.O. Box 9004, Abha 61413, Saudi Arabia*

<sup>5</sup>*Department of Mathematics, College of Science and Humanities in Al-Kharj,*

*Prince Sattam Bin Abdulaziz University, Al-Kharj 11942, Saudi Arabia*

Cavity optomagnetic platforms offer a promising route for exploring quantum phenomena, particularly quantum correlations, which are vital resources for modern quantum technologies. Here, we propose a theoretical scheme for achieving nonreciprocal quantum correlations such as entanglement, quantum discord, and Einstein-Podolsky-Rosen (EPR) via Barnett effect in a molecular-optomagnonical system, where a yttrium iron garnet sphere is placed in a microwave cavity that is hosting molecules. We show optimal parameter regimes for achieving nonreciprocal quantum correlations through Barnett effect. The generated entanglements are robust against thermal fluctuations, persisting even at temperatures as high as 6000K. Our scheme suggests a new tool for engineering noise-tolerant quantum correlations, and paves a way toward realizing novel nonreciprocal quantum devices by integrating magnons with molecular ensembles.

## I. INTRODUCTION

In magnetic crystals, the magnetic moments are generally not isolated. Their mutual interactions lead to collective excitations, referred to as spin waves (magnons) [1], which are commonly observed in ferrimagnetic materials such as yttrium iron garnet (YIG) sphere. Magnons have attracted significant attention due to their ability to couple strongly with microwave fields and various quantum systems. Interestingly, magnons can interact with lattice vibrations (phonons) via the magnetostrictive force [2], giving rise to cavity magnomechanics (CMM). This interaction enables the exploration of diverse phenomena and applications, including entanglement [3–5], quantum steering [6], ultrasensitive sensing [7], and ultraslow light propagation [8].

In recent years quantum correlations such as entanglement, quantum discord and EPR steering has been investigated in cavity optomechanical (COM) [6, 9–18], molecular optomechanical (McOM) [19–22], and cavity magnomechanical systems [23]. In particular, nonreciprocal entanglement in cavity optomechanical (COM) [24, 25], molecular optomechanical (McOM) [26], and cavity magnomechanical (CMM) systems [27] has attracted great interest. The ability to engineer nonreciprocal entanglement in these systems not only deepens our understanding of hybrid quantum systems but also opens up promising avenues for quantum information processing and plethora of quantum computational tasks [28]. While the Sagnac effect and chiral coupling [29] have been used to realize nonreciprocity in COM systems, mech-

anisms such as magnon Kerr nonlinearity [30] and Barnett effect [31] induce similar behaviour in CMM systems. This Barnett effect, discovered in 1915 [32], is a phenomenon where the rotation of an object with magnetic moments leads to magnetization. Nevertheless, the possibility of achieving nonreciprocal bipartite and tripartite entanglement, quantum discord and Einstein-Podolsky-Rosen (EPR) via the Barnett effect in a hybrid magnon-molecular system remains unexplored and will be the subject of our research.

In this work, we propose a theoretical scheme to generate and control nonreciprocal bipartite and tripartite entanglement, quantum discord and Einstein-Podolsky-Rosen (EPR) steering via the Barnett effect within a hybrid magnon-molecular system. This configuration features a spinning YIG sphere and ensemble of molecules placed in an optical cavity. The Barnett frequency shift of the magnon mode is induced by the rotation of the YIG sphere. This Barnett frequency shift can be turned from positive to negative by adjusting the direction of the rotation or bias magnetic field. This results in the generation of unidirectional entanglement, quantum discord and EPR steering. The underlying physical mechanism is that, due to the angular momentum conservation, the Barnett effect reverses the polarity of the induced magnetization when the bias magnetic field or the rotation direction is reversed, resulting in time-reversal symmetry breaking in the magnon-molecular system. Furthermore, our findings strikingly unveil a thermal robustness of our proposed magnon-molecular system. It maintains significant quantum correlations at temperatures approaching 6000 K. Finally, we demonstrate that perfect nonreciprocal bipartite and tripartite entanglement can be generated and controlled by exploring bidirectional contrast ratio. Our work paves a way for realizing novel nonreciprocal devices, and suggests a tool for engineering noise-tolerant quantum correlations.

\* [emale.kongkui@facsciences-uy1.cm](mailto:emale.kongkui@facsciences-uy1.cm)

† [djorwep@gmail.com](mailto:djorwep@gmail.com)

‡ [moabdalla@kku.edu.sa](mailto:moabdalla@kku.edu.sa)

§ [n.soopy@psau.edu.sa](mailto:n.soopy@psau.edu.sa)

The rest of our paper is structured as follows: Section II introduces the theoretical model and outlines the derivation of the dynamical equations. Section III delves into the numerical results and offers a thorough discussion of the underlying quantum correlations. Finally, Section IV provides concluding remarks.

## II. THEORETICAL MODEL AND DYNAMICAL EQUATIONS

Our benchmark system consists of a microwave cavity with frequency  $\omega_a$  that hosts a YIG sphere supporting a magnon mode with frequency  $\omega_m$  and a molecular mode with frequency  $\omega_\nu$  as sketched in Figure 1. Applying a bias magnetic field  $\mathbf{H}_0$  along the z-axis induces a uniform magnon mode in the sphere at the resonance frequency  $\omega_m = \gamma \mathbf{H}_0$ , with  $\gamma$  the gyromagnetic ratio. The rotating YIG sphere, with angular frequency  $\Delta_B$  generates an emergent magnetic field  $\mathbf{H}_B = \Delta_B/\gamma$  that induces a frequency shift in the magnon.

The Hamiltonian of the proposed system in the frame rotating at the driving frequency reads ( $\hbar = 1$ )

$$\begin{aligned} H = & \Delta_a a^\dagger a + (\Delta_m + \Delta_B) m^\dagger m + \sum_{j=1}^N \omega_\nu b_j^\dagger b_j \\ & + J(a^\dagger m + a m^\dagger) + \sum_{j=1}^N g_a a^\dagger a (b_j^\dagger + b_j) \\ & + \sum_{j=1}^N g_m m^\dagger m (b_j^\dagger + b_j) + i\mathcal{E}_l (m^\dagger + m) \end{aligned} \quad (1)$$

where  $a(a^\dagger)$ ,  $m(m^\dagger)$ , and  $b_j(b_j^\dagger)$  are the annihilation (creation) operators for the cavity mode  $a$ , magnon  $m$ , and the  $j$ -th individual molecular vibrational mode, respectively. The quantities  $\Delta_a = \omega_a - \omega_l$  and  $\Delta_m = \omega_m - \omega_l$  represent the frequency detuning of the cavity mode  $a$  and for magnon mode  $m$ . The magnon-photon coupling rate is captured by  $J$ , and  $g_a$  ( $g_m$ ) denotes the molecular-photon (molecular-magnon) coupling constant. The quantity  $\mathcal{E}_l = \gamma\sqrt{5\mathcal{N}}B_0/4$  denotes the coupling strength of the driving magnetic field with amplitude  $B_0$ , and  $\mathcal{N} = \rho V$  is the total number of spins, where  $\rho = 4.22 \times 10^{27} m^{-3}$ . Here,  $\rho$  is the spin density and  $V$  is the volume of the YIG sphere [2, 23, 33].

The above Hamiltonian can be simplified by introducing the molecular collective operator,  $B = \sum_{j=1}^N b_j/N$ , where  $[B, B^\dagger] = 1$ ,

and our Hamiltonian can be rewritten as,

$$\begin{aligned} H = & \Delta_a a^\dagger a + (\Delta_m + \Delta_B) m^\dagger m + \omega_\nu B^\dagger B + G_a a^\dagger a (B^\dagger + B) \\ & + G_m m^\dagger m (B^\dagger + B) + J(a^\dagger m + a m^\dagger) + i\mathcal{E}_l (m^\dagger + m), \end{aligned} \quad (2)$$

where  $G_a = g_a \sqrt{N}$  and  $G_m = g_m \sqrt{N}$  are the collective optomechanical coupling strengths.

## A. Quantum Langevin Equations and linearization

The evolution of the system in question is described by the set of quantum Langevin equations (QLEs),

$$\begin{cases} \dot{a} = & -(i\Delta_a + \kappa_a)a - iG_a a(B^\dagger + B) - iJm + \sqrt{2\kappa_a}a^{in}, \\ \dot{m} = & -(i(\Delta_m + \Delta_B) + \kappa_m)m - iG_m(B + B^\dagger) - iJa + \mathcal{E}_l \\ & + \sqrt{2\kappa_m}m^{in}, \\ \dot{B} = & -(i\omega_\nu + \gamma_\nu)B - iG_a a^\dagger a - iG_m m^\dagger m + \sqrt{2\gamma_\nu}B^{in}. \end{cases} \quad (3)$$

The noise operators  $a^{in}$ ,  $m^{in}$ , and  $B^{in}$ , where  $B^{in} = \frac{1}{\sqrt{N}} \sum_{j=1}^N b_j^{in}$  have zero mean values and are characterized by their following correlation functions,

$$\begin{cases} \langle a^{in}(t)a^{in\dagger}(t') \rangle = \delta(t - t'), \langle m^{in}(t)m^{in\dagger}(t') \rangle = \delta(t - t'), \\ \langle B^{in}(t)B^{in\dagger}(t') \rangle = (n_{th} + 1)\delta(t - t'), \\ \langle B^{in\dagger}(t)B^{in}(t') \rangle = n_{th}\delta(t - t'), \end{cases} \quad (4)$$

where  $n_{th} = [\exp(\hbar\omega_\nu/k_B T) - 1]^{-1}$  is the thermal phonon number for the mechanical mode at temperature  $T$ , and  $k_B$  is the Boltzmann constant. Considering a strong drive, the dynamics of our system can be linearized by splitting each operator into the sum of its steady-state mean value and a small fluctuation around it, i.e.  $\mathcal{O} = \langle \mathcal{O} \rangle + \delta\mathcal{O}$ , where  $\langle \mathcal{O} \rangle \equiv (\alpha, m_s, \beta)$  stands for the steady-state mean value and  $\delta\mathcal{O}$  captures the quantum fluctuation. Therefore, the linearized QLEs read,

$$\begin{cases} \delta\dot{a} = & -(i\tilde{\Delta}_a + \kappa_a)\delta a - iJ\delta m + \sqrt{2\kappa_a}a^{in}, \\ \delta\dot{m} = & -(i(\tilde{\Delta}_m + \Delta_B) + \kappa_m)\delta m - i\tilde{G}(\delta B + \delta B^\dagger) - iJ\delta a \\ & + \sqrt{2\kappa_m}m^{in}, \\ \delta\dot{B} = & -(i\omega_\nu + \gamma_\nu)\delta B - i\tilde{G}(\delta m^\dagger + \delta m) + \sqrt{2\gamma_\nu}B^{in}, \end{cases} \quad (5)$$

where  $\kappa_a$ ,  $\kappa_m$  and  $\gamma_\nu$  are the decay rates of the cavity mode, magnon mode and collective vibrational mode, respectively. We have also defined the following effective detunings  $\tilde{\Delta}_a = \Delta_a + 2G_a \text{Re}[\beta]$  and  $\tilde{\Delta}_m = \Delta_m + 2G_m \text{Re}[\beta]$ , together with their related effective couplings  $\tilde{G}_a = g_a |\alpha|$  and  $\tilde{G}_m = g_m |m_s|$ . In this work,  $\alpha$  and  $m_s$  are assumed to be a real numbers, as we can properly adjust the phase reference of the cavity fields. Similarly, the steady-state mean valued equations yield,

$$\begin{cases} \dot{\alpha} = & \frac{-iJm_s}{(i\tilde{\Delta}_a + \kappa_a)}, \quad m_s = \frac{\mathcal{E}_l - iJ\alpha}{(i(\tilde{\Delta}_m + \Delta_B) + \kappa_m)}, \\ \dot{\beta} = & \frac{-iG_a |\alpha|^2 - iG_m |m_s|^2}{i\omega_\nu + \gamma_\nu}. \end{cases} \quad (6)$$

To quantify quantum correlations, we define the following quantum quadratures operators,  $\delta X_o = \frac{(\delta o + \delta o^\dagger)}{\sqrt{2}}$ ,  $\delta Y_o = \frac{(\delta o - \delta o^\dagger)}{i\sqrt{2}}$  with ( $o \equiv a, m, B$ ), together with their corresponding noise operators, i.e.,  $X_o^{in} = \frac{(o^{in} + o^{in\dagger})}{\sqrt{2}}$ ,  $Y_o^{in} = \frac{(o^{in} - o^{in\dagger})}{i\sqrt{2}}$ . Therefore, our fluctuation dynamics in Eq. (5) can be written in a compact form as,

$$\dot{\mathbf{u}}(t) = A\mathbf{u}(t) + \mathbf{n}(t), \quad (7)$$

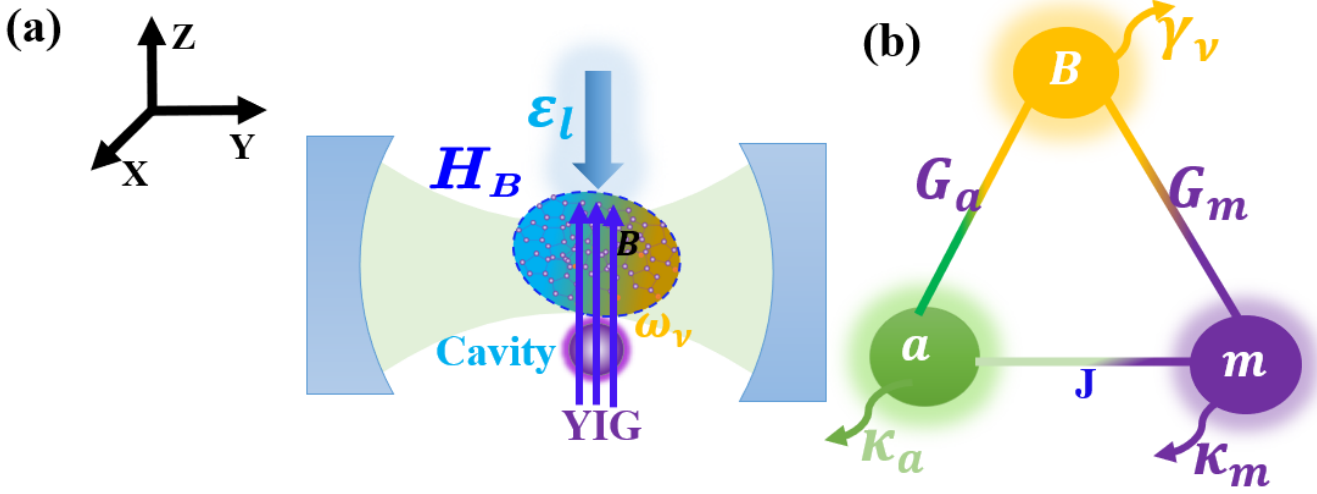


FIG. 1. (a) A magnon-molecular configuration featuring an ensemble of  $N$  identical molecules placed within a microwave cavity and a YIG sphere, with the magnon mode fully magnetized by the bias magnetic field  $\mathbf{H}_0$  (not shown). The rotating YIG sphere, with angular frequency  $\Delta_B$  generates an emergent magnetic field  $\mathbf{H}_B$  that induces a frequency shift in the magnon. (b) A schematic of the interaction picture illustrating the cavity-magnomechanical coupling between the cavity mode ( $a$ ) and magnon mode  $m$  as well as coupling between the magnon mode  $m$  and the collective molecular vibrational mode ( $B$ ).

with  $\mathbf{u}^\top = (\delta X_a, \delta Y_a, \delta X_m, \delta Y_m, \delta X_B, \delta Y_B)$ , and  $\mathbf{n}^\top = (\sqrt{2\kappa_a}X_a^{\text{in}}, \sqrt{2\kappa_a}Y_a^{\text{in}}, \sqrt{2\kappa_c}X_m^{\text{in}}, \sqrt{2\kappa_c}Y_m^{\text{in}}, \sqrt{2\gamma_m}X_B^{\text{in}}, \sqrt{2\gamma_m}Y_B^{\text{in}})$ . The drift matrix  $\mathbf{A}$  reads,

$$\mathbf{A} = \begin{pmatrix} -\kappa_a & \tilde{\Delta}_a & 0 & J & 0 & 0 \\ -\tilde{\Delta}_a & -\kappa_a & -J & 0 & -2\tilde{G}_a & 0 \\ 0 & J & -\kappa_m & \tilde{\Delta} & 0 & 0 \\ -J & 0 & -\tilde{\Delta} & -\kappa_m & -2\tilde{G}_m & 0 \\ 0 & 0 & 0 & 0 & -\gamma_\nu & \omega_\nu \\ -2\tilde{G}_a & 0 & -2\tilde{G}_m & 0 & -\omega_\nu & -\gamma_\nu \end{pmatrix}, \quad (8)$$

where  $\tilde{\Delta} = (\tilde{\Delta}_m + \Delta_B)$ . For our system to be stable, all real parts of the eigenvalues of the drift matrix  $\mathbf{A}$  must be negative. This essential stability condition is achieved using the Routh-Hurwitz criterion [34]. At this juncture, we introduce the covariance matrix  $\mathbf{V}$ , in order to explore the steady-state quantum correlations  $\mathbf{V}_{lk} = \frac{1}{2} \{ \langle \mathbf{u}_l(t) \mathbf{u}_k(t') \rangle + \langle \mathbf{u}_k(t') \mathbf{u}_l(t) \rangle \}$ . Equivalently, the elements of the covariance matrix  $\mathbf{V}$  can be also derived by numerically solving the following Lyapunov equation [35, 36],

$$\mathbf{AV} + \mathbf{VA}^\top = -\mathbf{D}, \quad (9)$$

where the diffusion matrix  $\mathbf{D}$ , which accounts for the influence of the noise operators, is given by,

$$\mathbf{D} = \text{diag} [\kappa_a, \kappa_a, \kappa_m, \kappa_m, \gamma_\nu(2n_{\text{th}} + 1), \gamma_\nu(2n_{\text{th}} + 1)]. \quad (10)$$

## B. Quantification of Bipartite and tripartite Entanglements

We employ the logarithmic negativity,  $E_n$  to quantify bipartite entanglement in our system. This is a

well-established entanglement monotone for Gaussian states [37]. Its mathematical expression is given by,

$$E_n = \max [0, -\ln(2\zeta)], \quad (11)$$

where,

$$\zeta \equiv \frac{1}{\sqrt{2}} \sqrt{\Sigma(V) - \sqrt{\Sigma(V)^2 - 4 \det(V)}}, \quad (12)$$

with  $\Sigma(V) = \det(\varphi_1) + \det(\varphi_2) - 2\det(\varphi_3)$ . For any given bipartite subsystem, the  $4 \times 4$  submatrix  $V_{\text{sub}}$  extracted from the full  $6 \times 6$  CM takes the canonical block form,

$$V_{\text{sub}} = \begin{pmatrix} \varphi_1 & \varphi_3 \\ \varphi_3^\top & \varphi_2 \end{pmatrix}, \quad (13)$$

where  $\varphi_1$  and  $\varphi_2$  are  $2 \times 2$  matrices representing each subsystem, and  $\varphi_3$  is a  $2 \times 2$  matrix encoding the correlations between the subsystems.

The minimum residual contangle  $\mathcal{R}_\tau^{\text{min}}$  is used to quantify tripartite quantum entanglement. It is defined as [38, 39],

$$\mathcal{R}_\tau^{\text{min}} \equiv \min [\mathcal{R}_\tau^{a|mB}, \mathcal{R}_\tau^{m|aB}, \mathcal{R}_\tau^{B|am}]. \quad (14)$$

This expression guarantees the invariance of tripartite entanglement under all possible permutations of the modes  $\mathcal{R}_\tau^{r|st} \equiv \mathcal{C}_{r|st} - \mathcal{C}_{r|s} - \mathcal{C}_{r|t}$ , ( $r, s, t \equiv a, m, B$ ), and it satisfies the monogamy of quantum entanglement  $\mathcal{R}_\tau^{r|st} \geq 0$ . Here,  $\mathcal{C}_{u|v}$  is the contangle of subsystem  $u$  and  $v$  ( $v$  contains one or two modes), which can be defined as squared logarithmic negativity and it is a proper entanglement monotone i.e.,  $\mathcal{C}_{u|v} = E_{N_{u|v}}^2$ , with  $E_N \equiv \max [0, -\ln 2\eta]$

, where  $\eta = \min \text{eig}[i\Omega_3\eta'_6]$ , with  $\Omega_3$  and  $\eta'_6$  defined respectively as,

$$\Omega_3 = \bigoplus_{k=1}^3 i\sigma_y, \quad \sigma_y = \begin{pmatrix} 0 & -i \\ i & 0 \end{pmatrix} \quad (15)$$

and,  $\eta'_6 = P_{r|st}V_6P_{r|st}$  for  $r, s, t \equiv a, m, B$ , where  $P_{a|mB} = \text{diag}(1, -1, 1, 1, 1, 1)$ ,  $P_{m|aB} = \text{diag}(1, 1, 1, -1, 1, 1)$ , and  $P_{B|am} = \text{diag}(1, 1, 1, 1, 1, -1)$  are partial transposition matrices and  $V_6$  is  $6 \times 6$  CM of the three modes.

### C. Gaussian Quantum Discord (GQD)

In order to realize a more comprehensive understanding of quantum correlations, we explore the Gaussian quantum discord (GQD). This quantity captures all forms of nonclassical correlations including those that exist even in separable states making it a valuable tool for quantum information tasks where entanglement alone is

not present [40, 41]. Consider a bipartite Gaussian subsystem  $l$ , characterized by its  $4 \times 4$  covariance matrix  $V_{\text{sub}}$ , the GQD is given by [41],

$$D_G^\ell = g(\sqrt{I_1^\ell}) - g(v_-^\ell) - g(v_+^\ell) + g(\sqrt{\mathcal{W}^\ell}), \quad (16)$$

where the function  $g(x)$  is defined as,

$$g(x) = \left( x + \frac{1}{2} \right) \ln \left( x + \frac{1}{2} \right) - \left( x - \frac{1}{2} \right) \ln \left( x - \frac{1}{2} \right). \quad (17)$$

The symplectic eigenvalues  $v_-^\ell$  and  $v_+^\ell$  of the subsystem's covariance matrix are obtained from,

$$v_\pm^\ell \equiv \frac{1}{\sqrt{2}} \left\{ \Sigma(V_{\text{sub}}^\ell) \pm [\Sigma(V_{\text{sub}}^\ell)^2 - 4I_4^\ell]^{1/2} \right\}^{1/2}, \quad (18)$$

with  $\Sigma(V_{\text{sub}}) = I_1^\ell + I_2^\ell + 2I_3^\ell$ . Here,  $I_1^\ell = \det(\varpi_1)$ ,  $I_2^\ell = \det(\varphi_2)$ ,  $I_3^\ell = \det(\varphi_3)$ , and  $I_4^\ell = \det(V_{\text{sub}})$ . The term  $\mathcal{W}^\ell$  is an important quantity that characterizes the quantumness of correlations and is given by [42],

$$\mathcal{W}^\ell = \begin{cases} \left( \frac{2|I_3^\ell| + \sqrt{4I_3^{\ell 2} + (4I_1^\ell - 1)(4I_4^\ell - I_2^\ell)}}{4I_1^\ell - 1} \right)^2 & \text{if } \frac{4(I_1^\ell I_2^\ell - I_4^\ell)^2}{(I_2^\ell + 4I_4^\ell)(1 + 4I_1^\ell)I_3^{\ell 2}} \leq 1, \\ \frac{I_1^\ell I_2^\ell + I_4^\ell - I_3^{\ell 2} - \sqrt{(I_1^\ell I_2^\ell + I_4^\ell - I_3^{\ell 2})^2 - 4I_1^\ell I_2^\ell I_4^\ell}}{2I_1^\ell} & \text{otherwise.} \end{cases} \quad (19)$$

An essential feature of the Gaussian states is that they exhibit entanglement if and only if their smallest symplectic eigenvalue  $v_-$  is less than  $1/2$ . This shows that while  $0 \leq D_G^\ell \leq 1$  can correspond to separable or entangled states, a value of  $D_G^\ell > 1$  definitively indicates an entangled state [41].

### D. Einstein-Podolsky-Rosen (EPR) steering

Apart from the entanglement, EPR steering captures a unique, directional type of quantum correlation, providing complementary insights into the non-classical properties of quantum systems. Quantum steering arises when measurements performed by one party (say Alice) can nonlocally define the quantum state held by another party (say Bob). The steerability from mode  $a$  to mode  $m$  ( $\mathcal{G}_{a \rightarrow m}$ ) and vice versa ( $\mathcal{G}_{m \rightarrow a}$ ) for Gaussian states can be quantified using the negativity-based measure introduced by Kogias *et al.* [43],

$$\mathcal{G}_{a \rightarrow m} = \max \left[ 0, \frac{1}{2} \ln \frac{\det V_a}{4 \det V_{am}} \right], \quad (20)$$

$$\mathcal{G}_{m \rightarrow a} = \max \left[ 0, \frac{1}{2} \ln \frac{\det V_m}{4 \det V_{am}} \right]. \quad (21)$$

where,  $V_a$  and  $V_m$  are  $2 \times 2$  covariance matrices of the modes  $a$  and  $m$ , respectively, and  $V_{am}$  is the  $4 \times 4$  covari-

ance matrix of the both modes  $a$  and  $m$ . It is necessary to note that while every steerable quantum state is necessarily entangled (non-separable), the reverse is not true, i.e., not all entangled states exhibit steerability. This distinction gives rise to different steering phenomena, i.e., no-way steering ( $\mathcal{G}_{a \rightarrow m} = \mathcal{G}_{m \rightarrow a} = 0$ ), one-way steering (e.g.,  $\mathcal{G}_{a \rightarrow m} > 0$  and  $\mathcal{G}_{m \rightarrow a} = 0$ ), and two-way steering ( $\mathcal{G}_{a \rightarrow m} > 0$  and  $\mathcal{G}_{m \rightarrow a} > 0$ ).

## III. RESULTS

In our numerical simulation, we have used the following experimentally feasible parameter [44–47], i.e.,  $\omega_\nu/2\pi = 30$  THz,  $\mathcal{E}_l/\omega_\nu = 3.8$ ,  $\gamma_\nu/\omega_\nu = 0.005$ ,  $g_\nu/\omega_\nu = 3.3 \times 10^{-6}$ ,  $\Delta_m/\omega_\nu = 1$ ,  $\Delta_a/\omega_\nu = -1$ ,  $|\Delta_B|/\omega_\nu = 0.3$ ,  $g_a = g_\nu$ ,  $g_m = g_\nu$ ,  $\kappa_a/\omega_\nu = 0.0166$ ,  $\kappa_a = \kappa_m$ ,  $J/\omega_\nu = 0.2$ , and  $T = 210$  K,  $N = 10^7$ , and  $T = 210$  K. Figure 2 represents the logarithmic negativity  $E_{ij}$  and the minimum residual contangle  $\mathcal{R}_\tau^{\min}$  as a function of the normalized detuning  $\tilde{\Delta}_a$  for different magnetic field direction. As it can be seen, the photon-magnon bipartite entanglement,  $E_{am}$ , is generated when  $-1 \leq \Delta_a \leq -0.5$  for  $-0.4 \leq \Delta_m \leq 0.4$  (see Figure 2(a)). More importantly, the photon-vibration entanglement  $E_{aB}$ , peaks around resonant condition i.e.,  $\tilde{\Delta}_a/\omega_\nu \sim -1$ . The underlying physical mechanism is that at resonance, the

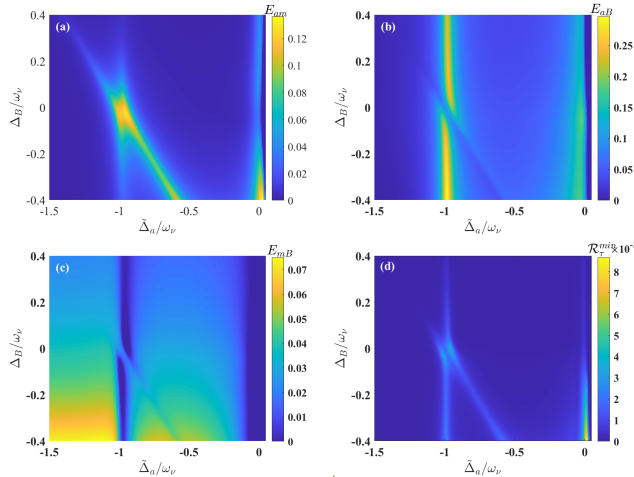


FIG. 2. Density plot of (a) bipartite entanglement for photon-magnon modes ( $E_{am}$ ), (b) bipartite entanglement for photon-vibration modes ( $E_{ab}$ ), (c) bipartite entanglement for magnon-vibration modes ( $E_{mb}$ ), and (d) the minimum residual cotangle  $\mathcal{R}_\tau^{\min}$  as a function of the normalized cavity detuning  $\tilde{\Delta}_a$  for different magnetic field direction. Common parameters for all subplots,  $\omega_\nu/2\pi = 30\text{THz}$ ,  $\mathcal{E}_l/\omega_\nu = 3.8$ ,  $\gamma_\nu/\omega_\nu = 0.005$ ,  $g_\nu/\omega_\nu = 3.3 \times 10^{-6}$ ,  $g_a = g_\nu$ ,  $g_m = g_\nu$ ,  $T = 210\text{K}$ ,  $\Delta_m/\omega_\nu = 1$ ,  $|\Delta_B|/\omega_\nu = 0.3$ ,  $\kappa_a/\omega_\nu = 0.0166$ ,  $\kappa_a = \kappa_m$ ,  $J/\omega_\nu = 0.2$ ,  $N = 10^7$ , and  $T = 210\text{K}$ .

entanglement initially generated between magnons and vibrations, arising from magnetoelastic interactions is subsequently redistributed to the photon-magnon and photon-vibration subsystems. Furthermore, after all the bipartite entanglements in the system are established, a tripartite entanglement among the photon, magnon, and vibrational modes emerges around resonance. This indicates that, under this resonant detuning condition, quantum correlations are not only present in the individual photon-magnon and photon-vibration pairs but also shared collectively among all three subsystems, forming a genuine three-mode entanglement (see Figure 2(d)).

In order to investigate nonreciprocal entanglement, we plot the three  $E_{ij}$  logarithmic negativities and the minimum residual contangle  $\mathcal{R}_\tau^{\min}$  as functions of the normalized cavity frequency detuning  $\tilde{\Delta}_a$  in Figure 3. When the YIG sphere rotates in a fixed direction, a magnetic field applied along z(-z) produces a positive (negative) frequency shift  $\Delta_B$  via the Barnett effect, similar to the Sagnac effect. Therefore, the Barnett effect can be used to break the time-reversal symmetry and realize unidirectional bipartite and tripartite entanglement in our system (see Figure 3). As shown in Figure 3, when the Barnett shift  $\Delta_B < 0$ , both bipartite and tripartite entanglements are enhanced, whereas they are dramatically suppressed when  $\Delta_B > 0$ , i.e., all the entanglements exhibit different responses when the direction of the magnetic field is reversed. This indicates that the sign of the Barnett-induced frequency shift plays a crucial role in controlling the strength of quantum correlations in the system, with

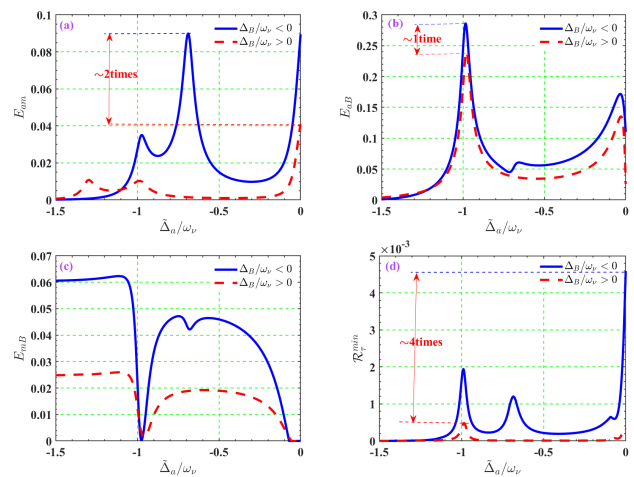


FIG. 3. (a) Plot of bipartite entanglement for photon-magnon modes ( $E_{am}$ ), (b) entanglement for vibration-photon modes ( $E_{ab}$ ), (c) entanglement for magnon-vibration modes ( $E_{mb}$ ), (d) minimum residual cotangle  $\mathcal{R}_\tau^{\min}$  as a function of the normalized detuning  $\tilde{\Delta}_a$ . The common parameters for these figures are,  $\omega_\nu/2\pi = 30\text{THz}$ ,  $\mathcal{E}_l/\omega_\nu = 3.8$ ,  $\gamma_\nu/\omega_\nu = 0.005$ ,  $g_\nu/\omega_\nu = 3.3 \times 10^{-6}$ ,  $T = 210\text{K}$ ,  $\tilde{\Delta}_m/\omega_\nu = 1$ ,  $|\Delta_B|/\omega_\nu = 0.3$ ,  $\kappa_a/\omega_\nu = 0.0166$ ,  $\kappa_a = \kappa_m$ ,  $J/\omega_\nu = 0.2$ ,  $N = 7$ , and  $T = 210\text{K}$ .

negative shifts favouring stronger entanglement and positive shifts weakening it. This allows the photon-magnon, photon-vibration, and tripartite entanglements to be enhanced by  $\sim 2$ ,  $1$ , and  $4$  times, respectively.

In Figure 4 displays the Gaussian Quantum Discord (GQD) against the normalized cavity detuning  $\tilde{\Delta}_a$ . The GQD exhibits nonreciprocal behaviour similar to that of the entanglement, responding differently when the direction of the applied magnetic field is reversed. As it can be seen on Figure 4, quantum correlation is strong when the Barnett frequency shift is negative ( $\Delta_B < 0$ ) and weak when  $\Delta_B > 0$ . Additionally, the photon-vibration and magnon-vibration quantum correlations are strong at resonance, i.e., when the cavity detuning is  $\tilde{\Delta}_a/\omega_\nu \sim -1$ . Among the different correlations, the photon-magnon correlation is the weakest, whereas the photon-vibration correlation is the strongest. The underlying physics behind this observation is that, since direct photon-magnon coupling  $J$  does not acquire the collective  $\sqrt{N}$  enhancement that amplifies the optomechanical and magnetoelastic interactions in the hybrid system, therefore, photon-magnon quantum discord remains weak. On the other hand, the photon-vibration and magnon-vibration correlations are greatly enhanced by cooperative,  $\sqrt{N}$ -scaled couplings.

Figure 5 shows a plot of one-way EPR steering as a function of normalized detuning  $\tilde{\Delta}_a$ . More interestingly, our system exhibits one-way EPR steering, where the vibrational mode acts as the only steering mode. EPR steering is found to occur exclusively from the vibrational mode  $B$  to the cavity mode  $a$  (see Figure 5(a))

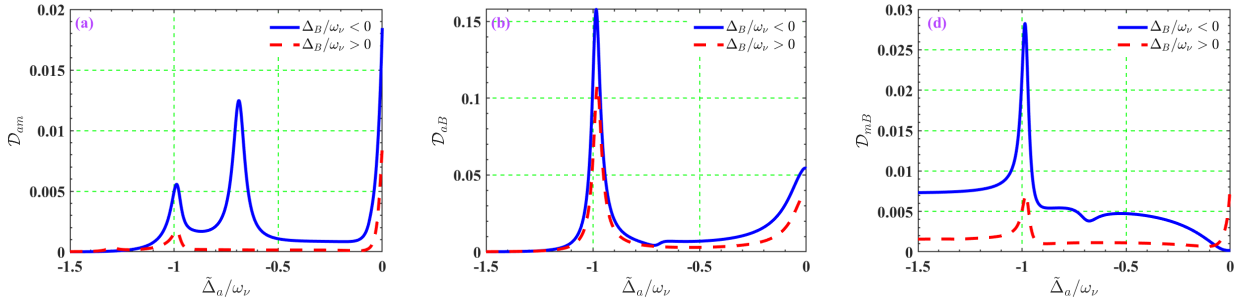


FIG. 4. (a) Plot of quantum discord for photon-magnon modes ( $D_{am}$ ). (b) Quantum discord for photon-vibration modes ( $D_{ab}$ ). (c) Quantum discord for magnon-vibration modes ( $D_{mb}$ ) as a function of detuning  $\Delta_a$ . The used parameters are,  $\omega_\nu/2\pi = 30\text{THz}$ ,  $\mathcal{E}_l/\omega_\nu = 3.8$ ,  $\gamma_\nu/\omega_\nu = 0.005$ ,  $g_\nu/\omega_\nu = 3.3 \times 10^{-6}$ ,  $T = 210\text{K}$ ,  $\Delta_m/\omega_\nu = 1$ ,  $|\Delta_B|/\omega_\nu = 0.3$ ,  $\kappa_a/\omega_\nu = 0.0166$ ,  $N = 7$ ,  $\kappa_a = \kappa_m$ , and  $J/\omega_\nu = 0.2$ .

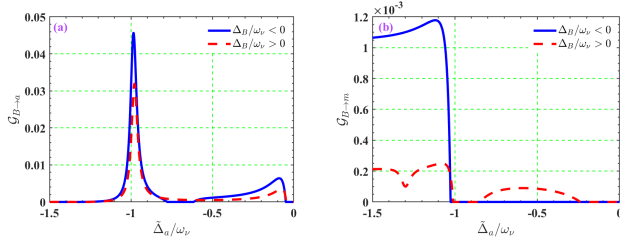


FIG. 5. (a) Plot of one-way steering  $\mathcal{G}_{B \rightarrow a}$ . (b) Plot of one-way steering  $\mathcal{G}_{B \rightarrow m}$  as a function of normalized detuning  $\tilde{\Delta}_a$ . The used parameters for these figures are,  $\omega_\nu/2\pi = 30\text{THz}$ ,  $\mathcal{E}_l/\omega_\nu = 3.8$ ,  $\gamma_\nu/\omega_\nu = 0.005$ ,  $g_\nu/\omega_\nu = 3.3 \times 10^{-6}$ ,  $T = 210\text{K}$ ,  $\Delta_m/\omega_\nu = 1$ ,  $|\Delta_B|/\omega_\nu = 0.3$ ,  $\kappa_a/\omega_\nu = 0.0166$ ,  $\kappa_a = \kappa_m$ ,  $J/\omega_\nu = 0.2$ ,  $N = 1 \times 10^7$  and  $T = 210\text{K}$ .

and from the vibrational mode  $B$  to the magnon mode  $m$  (see Figure 5(b)), with no observable steering between the photon and magnon modes in either direction. Particularly, when  $\Delta_B < 0$ , the steering from the vibrational mode to the cavity mode and from vibrational mode to the magnon mode is enhanced, whereas it is dramatically suppressed when the  $\Delta_B > 0$ . The underlying physics behind this phenomenon is that, the vibrational mode  $B$ , couples strongly to both the cavity mode and magnon mode via the enhanced couplings  $G_a$  and  $G_m$  respectively. This allows quantum information or correlations generated in  $B$  to be transferred to  $a$  and  $m$  enabling steering from  $B$  to  $a$  and from  $B$  to  $m$ . However, the direct photon-magnon coupling  $J$  is weak and lacks collective enhancement, so that the correlations between  $a$  and  $m$  are too small to produce steering in either direction. Thus, the system exhibits one-way EPR steering, where the vibrational mode acts as the only steering mode, and both the photon and magnon modes are steered but not steering.

Figure 6 depicts the nonreciprocal bipartite and tripartite entanglements as a function of molecular number  $N$ . The results reveal that all nonreciprocal entanglements increase generally with number of molecules  $N$ . As it can be seen in Figure 6, the photon-magnon  $E_{am}$  entangle-

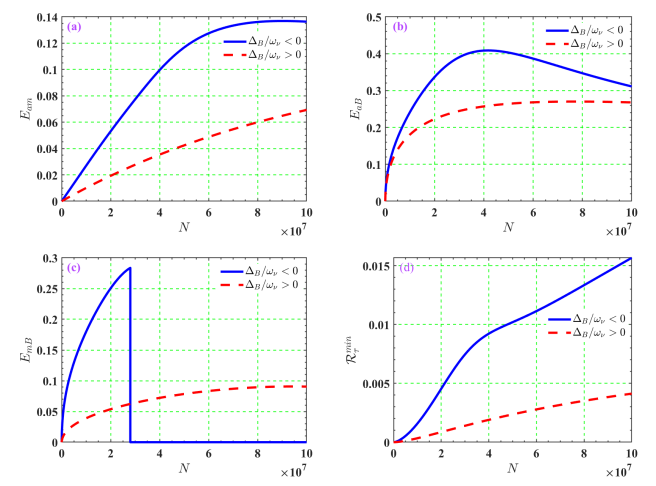


FIG. 6. (a) Photon-magnon entanglement  $E_{am}$  vs number of molecules  $N$ . (b) Photon-vibration entanglement  $E_{ab}$  vs number of molecules  $N$ . (c) Entanglement for magnon-vibration modes ( $E_{mb}$ ) with  $\Delta_m/\omega_\nu = 0.5$  and  $\Delta_a/\omega_\nu = -0.5$  as a function of number of molecules  $N$ . (d) Minimum residual cotangle  $\mathcal{R}^{min}$  with  $\Delta_m/\omega_\nu = 1$  and  $\Delta_a/\omega_\nu = -1$  as a function of number of molecules  $N$ . The other used parameters are,  $\omega_\nu/2\pi = 30\text{THz}$ ,  $\mathcal{E}_l/\omega_\nu = 3.8$ ,  $\gamma_\nu/\omega_\nu = 0.005$ ,  $g_\nu/\omega_\nu = 3.3 \times 10^{-6}$ ,  $T = 210\text{K}$ ,  $\tilde{\Delta}_a/\omega_\nu = -1$ ,  $\Delta_m/\omega_\nu = 1$ ,  $|\Delta_B|/\omega_\nu = 0.3$ ,  $\kappa_a/\omega_\nu = 0.0166$ ,  $\kappa_a = \kappa_m$ ,  $J/\omega_\nu = 0.2$ , and  $T = 210\text{K}$ .

ment also grows with  $N$  but its value remains smaller than those of photon-vibration and magnon-vibration entanglements. The increase in photon-vibration and magnon-vibration entanglements arises because  $E_{ab}$  and  $E_{mb}$  are monotonically increasing function of the collective coupling strength  $G_a = g_a\sqrt{N}$  and  $G_m = g_m\sqrt{N}$ . In contrast, the direct photon-magnon coupling  $J$  does not benefit from such collective enhancement, limiting the magnitude of  $E_{am}$  as  $N$  increases.

In Figure 7, we display the robust nonreciprocal bipartite and tripartite entanglements against temperature. Our findings strikingly unveil the highly thermal robustness of the proposed magnon-molecular hybrid system.

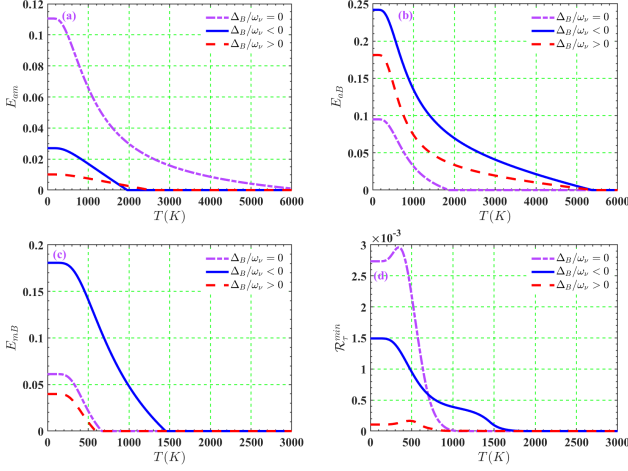


FIG. 7. (a) Plot of bipartite entanglement for photon-magnon modes ( $E_{am}$ ). (b) Entanglement for vibration-photon modes ( $E_{ab}$ ). (c) Entanglement for magnon-vibration modes ( $E_{mb}$ ) with  $\Delta_m/\omega_\nu = 0.5$  and  $\Delta_a/\omega_\nu = -0.5$  as a function of temperature  $T$ . (d) Minimum residual cotangle  $\mathcal{R}_\tau^{\min}$  with  $\Delta_m/\omega_\nu = 0.5$  and  $\Delta_a/\omega_\nu = -0.5$  as a function of temperature  $T$ . Common parameters for all subplots are,  $\omega_\nu/2\pi = 30\text{THz}$ ,  $\mathcal{E}_l/\omega_\nu = 3.8$ ,  $\gamma_\nu/\omega_\nu = 0.005$ ,  $g_\nu/\omega_\nu = 3.3 \times 10^{-6}$ ,  $T = 210\text{K}$ ,  $\tilde{\Delta}_a/\omega_\nu = -1$ ,  $\Delta_m/\omega_\nu = 1$ ,  $|\Delta_B|/\omega_\nu = 0.3$ ,  $\kappa_a/\omega_\nu = 0.0166$ ,  $\kappa_a = \kappa_m$ ,  $J/\omega_\nu = 0.2$ ,  $N = 10^7$  and  $T = 210\text{K}$ .

Unlike conventional optomechanical and magnomechanical systems, which lose coherence rapidly at elevated temperatures, our setup retains significant quantum correlations even at temperatures approaching 6000 K. This remarkable resilience can be attributed to the high frequency vibrations of the molecules, which arise from their collective nature. Consequently, entanglement remains largely unaffected by thermal noise, allowing the system to maintain coherent quantum behavior in regimes where conventional optomechanical and magnomechanical systems would be completely uncorrelated. This makes the magnon-molecular platform highly promising for robust high-temperature quantum technologies, where strong correlations can survive at room temperatures.

### A. Switchable nonreciprocity

Here, we use the following bidirectional contrast ratio  $\mathcal{C}_{ij}$  ( $\mathcal{C}_\mathcal{R}$ ) for bipartite (tripartite) entanglement to quantitatively describe nonreciprocal entanglement [27],

$$\mathcal{C}_{ij} = \frac{|E_{ij}(\Delta_B > 0) - E_{ij}(\Delta_B < 0)|}{E_{ij}(\Delta_B > 0) + E_{ij}(\Delta_B < 0)}, \quad (22)$$

$$\mathcal{C}_\mathcal{R} = \frac{|\mathcal{R}_\tau^{\min}(\Delta_B > 0) - \mathcal{R}_\tau^{\min}(\Delta_B < 0)|}{\mathcal{R}_\tau^{\min}(\Delta_B > 0) + \mathcal{R}_\tau^{\min}(\Delta_B < 0)}.$$

From these definitions, the bidirectional contrast ratio satisfies the condition  $0 \leq \mathcal{C} \leq 1$ . These bidirectional contrasts provide quantitative measure of nonreciprocal

entanglement, i.e., the closer they approach to unity, the more pronounced the entanglement is asymmetric between the interacting modes. We numerically plot the contrast ratio versus the normalized detuning  $\tilde{\Delta}_a/\omega_\nu$  in Figure 8(a) to clearly demonstrate this behaviour. It can be observed from Figure 8(a) that the nonreciprocity of both bipartite and tripartite entanglements can be switched on or off by tuning the cavity detuning  $\tilde{\Delta}_a/\omega_\nu$ . Furthermore, the bidirectional contrast ratios for all entanglements (except for magnon-vibration entanglement,  $E_{mb}$ ) can be tuned continuously from 0 to 1 by adjusting the cavity detuning  $\tilde{\Delta}_a/\omega_\nu$ . All entanglements in our system become perfectly nonreciprocal as the frequency detuning is adjusted, except for the magnon-vibration pair, which retains partial reciprocity because the magnon-vibration coupling channel is less affected by the cavity detuning  $\tilde{\Delta}_a$ . It can be also seen from Figure 8(b) that perfect nonreciprocity can be achieved by varying the normalized magnon detuning  $\tilde{\Delta}_m$ . Our findings show that perfect nonreciprocity of photon-magnon entanglement can be achieved with the system in question when the temperature  $T > 2000\text{K}$  (see Figure 8(c)). Similarly nonreciprocity of tripartite entanglement is achieved when  $840\text{K} \leq T \leq 1864\text{K}$ . These observations reveal how noise-tolerant quantum correlations can be engineered in our proposal. Such nonreciprocal robust quantum resources are useful for quantum quantum processing, and plethora modern quantum computational tasks.

### B. Experimental feasibility

The proposed magnon-molecular hybrid system can be realized experimentally, using currently available experimental techniques in cavity optomagnonics, cavity magnomechanics and molecular cavity quantum electrodynamics. To realize this setup, the magnon mode can be implemented using a YIG sphere placed inside a microwave cavity. Strong photon-magnon coupling with rates on the order of  $\sim 90\text{ MHz}$  has already been demonstrated experimentally [48, 49], enabling coherent magnon-photon interactions. The molecular ensemble can be introduced by embedding or coating a layer of molecules on or near the YIG sphere surface, or by placing them inside the same microwave cavity mode volume [50]. The molecular ensemble supports collective vibrational excitations that can couple to both the cavity field and the magnon mode via radiation pressure or magnetostrictive interactions. Since the effective coupling strengths scale as  $G_{a,m} = g_{a,m}\sqrt{N}$ , even moderate single-molecule coupling can lead to strong collective interactions for large (typically  $10^6$ – $10^{10}$  molecules), which is feasible using dense molecular films. The Barnett frequency shift  $\Delta_B$  of the magnon mode can be controlled by adjusting the rotation or magnetization of the YIG sphere. Previous experiments have demonstrated controlled mechanical rotation of YIG spheres by attaching them to rotors or air turbines, achieving angular frequen-

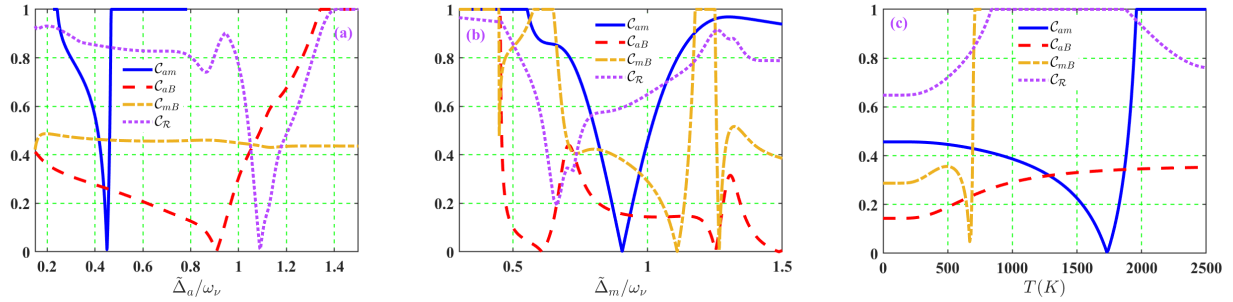


FIG. 8. (a) Plot of bidirectional contrast ratio  $\mathcal{C}_{am}$ ,  $\mathcal{C}_{aB}$ ,  $\mathcal{C}_{mB}$  and  $\mathcal{C}_{R}$  as a function of cavity detuning  $\tilde{\Delta}_a$ . (b) bidirectional contrast ratio  $\mathcal{C}_{am}$ ,  $\mathcal{C}_{aB}$ ,  $\mathcal{C}_{mB}$  and  $\mathcal{C}_{R}$  as a function of magnon detuning  $\tilde{\Delta}_m$ . (c) bidirectional contrast ratio  $\mathcal{C}_{am}$ ,  $\mathcal{C}_{aB}$ ,  $\mathcal{C}_{mB}$  and  $\mathcal{C}_{R}$  as a function of temperature T. The used parameters for these figures are,  $\omega_\nu/2\pi = 30\text{THz}$ ,  $\mathcal{E}_l/\omega_\nu = 3.8$ ,  $\gamma_\nu/\omega_\nu = 0.005$ ,  $g_\nu/\omega_\nu = 3.3 \times 10^{-6}$ ,  $T = 210\text{K}$ ,  $\Delta_m/\omega_\nu = 1$ ,  $\tilde{\Delta}_a/\omega_\nu = 1$ ,  $|\Delta_B|/\omega_\nu = 0.3$ ,  $\kappa_a/\omega_\nu = 0.0166$ ,  $\kappa_a = \kappa_m$ ,  $J/\omega_\nu = 0.2$ ,  $N = 10^7$ , and  $T = 210\text{K}$ .

cies of several kilohertz and even reaching gigahertz-scale rotation using levitated nanoparticles [31, 51, 52]. In our system, this tunable Barnett shift directly influences the direction dependent quantum correlations and can thus be used as a practical control knob. Potential experimental challenges here include maintaining low electromagnetic background noise in electrically driven systems and controlling temperature fluctuations in the rotating YIG sphere. However, experimental data show that frequency fluctuations on the order of  $\pm 30$  Hz at rotation frequencies of a few kilohertz are negligible, and the associated temperature variations ( $\sim 0.1$  K) are minimal [31, 32, 53, 54]. Therefore, given the demonstrated capabilities in magnomechanical systems and the well-established control of molecular vibrational modes in cavity electrodynamics (QED), the realization of our proposed magnon-molecular system is experimentally feasible with current or near-future technology.

#### IV. CONCLUSION

In summary, we have investigated the generation of fundamental quantum correlations specifically entanglement, EPR steering, and quantum discord within a magnon-molecular system. Our findings demonstrate nonreciprocal entanglement, quantum and EPR steering can be generated and control via the Barnett frequency shift  $\Delta_B$ . All the quantum corrections are enhanced when  $\Delta_B < 0$  and dramatically suppressed when  $\Delta_B > 0$ . Furthermore, by appropriately tuning the system parameters, perfect nonreciprocity of bipartite and tripartite entanglement can be achieved with our system. More interestingly, the generated entanglements demonstrate remarkable thermal robustness, remaining significant even at temperatures approaching 6000 K. This exceptional resilience originates from the collective and high-frequency vibrational nature of the molecular ensemble, which leads to strong effective coupling strengths that dominate over thermal noise. Consequently, our re-

sults suggest that the proposed magnon-molecular system provides a promising platform for realizing high-temperature quantum information processing and quantum sensing, where robust and tunable nonreciprocal entanglement can be harnessed without the need for cryogenic cooling.

#### ACKNOWLEDGMENTS

P.D. acknowledges the Iso-Lomso Fellowship at Stellenbosch Institute for Advanced Study (STIAS), Wallenberg Research Centre at Stellenbosch University, Stellenbosch 7600, South Africa, and The Institute for Advanced Study, Wissenschaftskolleg zu Berlin, Wallotstrasse 19, 14193 Berlin, Germany. The authors extend their appreciation to the Deanship of Research and Graduate Studies at King Khalid University for funding this work through Large Research project under grant number RGP2/678/46. The authors are thankful to the Deanship of Graduate Studies and Scientific Research at University of Bisha for supporting this work through the Fast-Track Research Support Program.

#### AUTHOR CONTRIBUTIONS

E.K.B. and P.D. conceptualized the work and carried out the simulations and analysis. A.-H. A.-A. and P.D. participated in all the discussions and provided useful methodology and suggestions for the final version of the manuscript. M.A. and K.S.N. participated in the discussions and supervised the work. All authors participated equally in the writing, discussions, and the preparation of the final version of the manuscript.

#### COMPETING INTERESTS

All authors declare no competing interests.

## DATA AVAILABILITY

Relevant data are included in the manuscript and supporting information. Supplementary data are available upon reasonable request.

---

[1] D. D. Stancil and A. Prabhakar, *Spin waves: problems and solutions* (Springer Nature, 2021) pp. 21–35.

[2] C. A. Potts, E. Varga, V. A. S. V. Bittencourt, S. V. Kusminskiy, and J. P. Davis, Dynamical backaction magnomechanics, *Phys. Rev. X* **11**, 031053 (2021).

[3] B. Hussain, S. Qamar, and M. Irfan, Entanglement enhancement in cavity magnomechanics by an optical parametric amplifier, *Phys. Rev. A* **105**, 063704 (2022).

[4] W. Qiu, X. Cheng, A. Chen, Y. Lan, and W. Nie, Controlling quantum coherence and entanglement in cavity magnomechanical systems, *Phys. Rev. A* **105**, 063718 (2022).

[5] A. Sohail, R. Ahmed, J.-X. Peng, A. Shahzad, and S. K. Singh, Enhanced entanglement via magnon squeezing in a two-cavity magnomechanical system, *J. Opt. Soc. Am. B* **40**, 1359 (2023).

[6] X. Ge, J.-X. Peng, and Y.-Y. Chen, Entanglement and steering in a three-dimensional cavity magnomechanics system, *Phys. Rev. A* **111**, 023710 (2025).

[7] M. F. Colombano, G. Arregui, F. Bonell, N. E. Capuji, E. Chavez-Angel, A. Pitanti, S. O. Valenzuela, C. M. Sotomayor-Torres, D. Navarro-Urrios, and M. V. Costache, Ferrromagnetic resonance assisted optomechanical magnetometer, *Phys. Rev. Lett.* **125**, 147201 (2020).

[8] T.-X. Lu, X. Xiao, L.-S. Chen, Q. Zhang, and H. Jing, Magnon-squeezing-enhanced slow light and second-order sideband in cavity magnomechanics, *Phys. Rev. A* **107**, 063714 (2023).

[9] J. Huang, D. Lai, and J.-Q. Liao, Thermal-noise-resistant optomechanical entanglement via general dark-mode control (2022).

[10] S. M. Tchounda, P. Djorwé, S. N. Engo, and B. Djafari-Rouhani, Sensor sensitivity based on exceptional points engineered via synthetic magnetism, *Physical Review Applied* **19**, 10.1103/PhysRevApplied.19.064016 (2023).

[11] D. Massembele, P. Djorwé, K. Emale, J.-X. Peng, A.-H. Abdel-Aty, and K. Nisar, Low threshold quantum correlations via synthetic magnetism in brillouin optomechanical system, *Physica B: Condensed Matter* **697**, 416689 (2025).

[12] A. Sohail, M. Amazioug, S. K. Singh, N. Chabar, R. Ahmed, and M. C. de Oliveira, Coherent feedback control of indirectly coupled mode multipartite entanglement in a cavity opto-magnomechanical system, *Annalen der Physik* **10.1002/andp.202400375** (2025).

[13] F. Bemani, R. Roknizadeh, A. Motazedifard, M. H. Naderi, and D. Vitali, Quantum correlations in optomechanical crystals, *Phys. Rev. A* **99**, 063814 (2019).

[14] C. Shang and H. Li, Resonance-dominant optomechanical entanglement in open quantum systems, *Phys. Rev. Appl.* **21**, 044048 (2024).

[15] D. R. K. Massembele, P. Djorwe, A. K. Sarma, A.-H. Abdel-Aty, and S. G. N. Engo, Quantum entanglement assisted via duffing nonlinearity, *Physical Review A: Atomic, Molecular, and Optical Physics* **110**, 043502 (2024).

[16] K. Emale, J.-X. Peng, P. Djorwe, A. Sarma, Abdourahimi, A.-H. Abdel-Aty, K. Nisar, and S. Engo, Quantum correlations enhanced in hybrid optomechanical system via phase tuning, *Physica B: Condensed Matter* **701**, 416919 (2025).

[17] P. Djorwe, A.-H. Abdel-Aty, K. Nisar, and S. Engo, Optomechanical entanglement induced by backward stimulated brillouin scattering, *Optik* **319**, 172097 (2024).

[18] P. Chen, D.-W. Luo, and T. Yu, Optimal entanglement generation in optomechanical systems via krotov control of covariance matrix dynamics, *Physical Review Research* **7**, 013161 (2025).

[19] J. Huang, D. Lei, G. S. Agarwal, and Z. Zhang, Collective quantum entanglement in molecular cavity optomechanics, *Physical Review B* **110**, 184306 (2024).

[20] E. K. Berinyuy, C. Tchodimou, P. Djorwe, A.-H. Abdel-Aty, K. S. Nisar, and S. G. N. Engo, Enhancing mechanical entanglement in molecular optomechanics, *The European Physical Journal Plus* **140**, 10.1140/epjp/s13360-025-06741-y (2025).

[21] E. K. Berinyuy, D. R. K. Massembele, P. Djorwe, R. Altuijri, A. H. Abdel-Aty, and S. G. N. Engo, *Quantum correlations in molecular cavity optomechanics* (2025), arXiv:2506.07277 [quant-ph].

[22] E. K. Berinyuy, C. Tchodimou, P. Djorwé, S. K. Singh, and S. G. N. Engo, *A blueprint for robust, high-temperature quantum entanglement with pt-symmetric molecular optomechanics* (2025), arXiv:2509.16675 [quant-ph].

[23] J. Li, S.-Y. Zhu, and G. Agarwal, Magnon-phonon-phonon entanglement in cavity magnomechanics, *Physical Review Letters* **121**, 10.1103/PhysRevLett.121.203601 (2018).

[24] Y.-F. Jiao, J.-X. Liu, Y. Li, R. Yang, L.-M. Kuang, and H. Jing, Nonreciprocal enhancement of remote entanglement between nonidentical mechanical oscillators, *Physical Review Applied* **18**, 10.1103/PhysRevApplied.18.064008 (2022).

[25] Y.-F. Jiao, S.-D. Zhang, Y.-L. Zhang, A. Miranowicz, L.-M. Kuang, and H. Jing, Nonreciprocal optomechanical entanglement against backscattering losses, *Physical Review Letters* **125**, 10.1103/PhysRevLett.125.143605 (2020).

[26] E. K. Berinyuy, J.-X. Peng, A. Sohail, P. Djorwé, A.-H. Abdel-Aty, N. Alessa, K. Nisar, and S. N. Engo, Nonreciprocal entanglement in a molecular optomechanical system, *Physica B: Condensed Matter* **713**, 417313 (2025).

[27] J. Chen, X.-G. Fan, W. Xiong, D. Wang, and L. Ye, Nonreciprocal entanglement in cavity-magnon optomechanics, *Phys. Rev. B* **108**, 024105 (2023).

[28] F. Xu, X. Ma, Q. Zhang, H.-K. Lo, and J.-W. Pan, Secure quantum key distribution with realistic devices, *Rev.*

Mod. Phys. **92**, 025002 (2020).

[29] T.-X. Lu, B. Li, Y. Wang, D.-Y. Wang, X. Xiao, and H. Jing, Directional quantum-squeezing-enabled nonreciprocal enhancement of entanglement, Phys. Rev. Appl. **22**, 064001 (2024).

[30] J. Chen, X.-G. Fan, W. Xiong, D. Wang, and L. Ye, Nonreciprocal photon-phonon entanglement in kerr-modified spinning cavity magnomechanics, Phys. Rev. A **109**, 043512 (2024).

[31] T.-X. Lu, Z.-S. Li, L.-S. Chen, Y. Wang, X. Xiao, and H. Jing, Nonreciprocal entanglement in cavity magnomechanics via the barnett effect, Phys. Rev. A **111**, 013713 (2025).

[32] S. J. Barnett, Magnetization by rotation, Phys. Rev. **6**, 239 (1915).

[33] Z. Shen, G.-T. Xu, M. Zhang, Y.-L. Zhang, Y. Wang, C.-Z. Chai, C.-L. Zou, G.-C. Guo, and C.-H. Dong, Coherent coupling between phonons, magnons, and photons, Phys. Rev. Lett. **129**, 243601 (2022).

[34] E. X. DeJesus and C. Kaufman, Routh-hurwitz criterion in the examination of eigenvalues of a system of nonlinear ordinary differential equations, Phys. Rev. A **35**, 5288 (1987).

[35] C. W. Gardiner and P. Zoller, *Quantum Noise* (Springer Berlin Heidelberg, 2000).

[36] G. Vidal and R. F. Werner, Computable measure of entanglement, Physical Review A **65**, 032314 (2002).

[37] M. B. Plenio, Logarithmic negativity: A full entanglement monotone that is not convex, Phys. Rev. Lett. **95**, 090503 (2005).

[38] G. Adesso and F. Illuminati, Continuous variable tangle, monogamy inequality, and entanglement sharing in gaussian states of continuous variable systems, New Journal of Physics **8**, 15 (2006).

[39] G. Adesso and F. Illuminati, Entanglement in continuous-variable systems: recent advances and current perspectives, Journal of Physics A: Mathematical and Theoretical **40**, 7821 (2007).

[40] H. Ollivier and W. H. Zurek, Quantum discord: A measure of the quantumness of correlations, Physical Review Letters **88**, 017901 (2001).

[41] P. Giorda and M. G. A. Paris, Gaussian quantum discord, Phys. Rev. Lett. **105**, 020503 (2010).

[42] S. Chakraborty and A. K. Sarma, Enhancing quantum correlations in an optomechanical system via cross-kerr nonlinearity, J. Opt. Soc. Am. B **34**, 1503 (2017).

[43] I. Kogias, A. R. Lee, S. Ragy, and G. Adesso, Quantification of gaussian quantum steering, Phys. Rev. Lett. **114**, 060403 (2015).

[44] Z. Koczor-Benda, P. Roelli, C. Galland, and E. Rosta, Molecular vibration explorer: an online database and toolbox for surface-enhanced frequency conversion and infrared and raman spectroscopy, The Journal of Physical Chemistry A **126**, 4657 (2022).

[45] R. Chikkaraddy, A. Xomalis, L. A. Jakob, and J. J. Baumberg, Publisher correction: Mid-infrared-perturbed molecular vibrational signatures in plasmonic nanocavities, Light, Science & Applications **11**, 41 (2022).

[46] F. Zou, L. Du, Y. Li, and H. Dong, Amplifying frequency up-converted infrared signals with a molecular optomechanical cavity, Phys. Rev. Lett. **132**, 153602 (2024).

[47] P. Roelli, H. Hu, E. Verhagen, S. Reich, and C. Galland, Nanocavities for molecular optomechanics: Their fundamental description and applications, ACS Photonics **11**, 4486 (2024).

[48] B. Bhoi, B. Kim, J. Kim, Y.-J. Cho, and S.-K. Kim, Robust magnon-photon coupling in a planar-geometry hybrid of inverted split-ring resonator and yig film, Scientific reports **7**, 11930 (2017).

[49] V. A. Bittencourt, C. Potts, J. Davis, and A. Metelmann, Magnon-microwave backaction noise evasion in cavity magnomechanics, Communications Physics **8**, 247 (2025).

[50] A. Shalabney, J. George, J. a. Hutchison, G. Pupillo, C. Genet, and T. W. Ebbesen, Coherent coupling of molecular resonators with a microcavity mode, Nature Communications **6**, 5981 (2015).

[51] R. Reimann, M. Doderer, E. Hebestreit, R. Diehl, M. Frimmer, D. Windey, F. Tebbenjohanns, and L. Novotny, Ghz rotation of an optically trapped nanoparticle in vacuum, Phys. Rev. Lett. **121**, 033602 (2018).

[52] M. Schuck, D. Steinert, T. Nussbaumer, and J. W. Kolar, Ultrafast rotation of magnetically levitated macroscopic steel spheres, Science advances **4**, e1701519 (2018).

[53] M. Ono, H. Chudo, K. Harii, S. Okayasu, M. Matsuo, J. Ieda, R. Takahashi, S. Maekawa, and E. Saitoh, Barnett effect in paramagnetic states, Phys. Rev. B **92**, 174424 (2015).

[54] S. Bretzel, G. E. Bauer, Y. Tserkovnyak, and A. Brataas, Barnett effect in thin magnetic films and nanostructures, Applied Physics Letters **95** (2009).